PHYSICAL REVIEW B VOLUME 33, NUMBER 5 1 MARCH 1986

Magnetic properties of superlattices formed from ferromagnetic and antiferromagnetic materials

L. L. Hinchey and D. L. Mills
Department of Physics, University of California, Irvine, California 92717
(Received 30 September 1985)

We present theoretical studies of basic magnetic response characteristics of superlattice structures formed from alternating layers of ferromagnetic and antiferromagnetic materials, each described through use of a localized spin model. The geometry explored here is one in which the antiferromagnet consists of sheets parallel to each interface within which the spins are aligned ferromagnetically. The study of the classical (mean-field) ground state as a function of magnetic field shows that a sequence of spin-reorientation transitions occur, particularly for superlattices within which the antiferromagnetic constituent consists of an even number of layers. For the various phases, we present calculations of the spin-wave spectrum, and also the infrared absorption spectrum.

I. INTRODUCTION

An exciting aspect of solid-state physics is the discovery or exploration of new classes of materials, whose physical properties may differ dramatically from textbook descriptions of simple solids. During the past decade, there has been considerable effort devoted to the synthesis and study of composite materials, and of superlattices formed from alternating layers of different materials. One may create new materials in the laboratory, with properties distinct from those of any single constituent.

Superlattices of extraordinary quality may be formed from semiconducting materials. In these samples, the boundary between adjacent materials is perfectly sharp, on the atomic scale. These systems also have been studied in great detail. Superlattices may also be formed from a variety of other materials, and while the sample quality at present is inferior to that realized with semiconductors, we see the appearance of superlattices formed from new combinations of materials, and the sample quality (e.g., the sharpness of the interfaces between adjacent media) is improving steadily.

From superlattice structures made from magnetic materials, one can fabricate materials with microwave or infrared response characteristics subject to design. As we shall see, such systems have intriguing physical properties, in that for certain geometries magnetic-field-induced spin-reorientation transitions may occur for externally applied magnetic fields of modest magnitudes.

In magnetic superlattices, elementary excitations such as spin waves are collective excitations of the structure as a whole, and as a consequence have properties distinctly different from the modes associated with any one constituent. We have one example in hand where collective excitations unique to a magnetic superlattice have been studied experimentally. Schuller and collaborators have fabricated superlattices from alternating films on Ni and Mo, the thickness of each film can range from 100 Å to several hundred angstroms.[1] In an isolated Ni film placed in a static Zeeman field H_0 parallel to its surface, there are surface spin waves which propagate along either the upper or lower surface. In the long-wavelength limit, these are the waves discussed many years ago by Damon and Eshbach.[2] Their excitation energy receives its dominant contribution from the Zeeman and dipolar interactions at the long wavelengths studied so far. In a superlattice, surface spin waves on different Ni films may interact through the dipole fields generated by the spin motion, and this leads to new modes that are collective excitations of the superlattice structure as a whole, and which may transmit energy normal to the interfaces between the films.[3,4] If the superlattice is terminated, and only if the thickness d_1 of the Ni films is greater than that of d_2 of the Mo film, one realizes a surface mode of the superlattice structure as a whole, which is in fact a linear combination of surface waves in each Ni film.[3,4] The mode has been studied by the method of Brillouin scattering of light, and its properties correlate nicely with the earlier theoretical predictions.

A rich variety of behaviors may be expected if one forms superlattices from alternating layers of ferromagnetic and antiferromagnetic material. This paper is devoted to a theoretical study of the properties of superlattices formed from such materials, and our theoretical model exhibits rich behavior. We have no specific combinations of materials in mind from which one may realize an analogue of the model system studied here. Our intent is to present a basic theoretical study of the class of phenomena one may encounter in such systems.

For selected structures, one can easily appreciate that interesting spin-reorientation transitions can occur in rather low externally applied fields. Consider the case (the only geometry considered in the present paper) where the antiferromagnet consists of sheets of spins within which there is ferromagnetic alignment of the moments. Then form a superlattice from alternating layers of ferromagnetic and antiferromagnetic material. For the moment, let the antiferromagnetic constituent consist of an *even* number of layers, with ferromagnetic coupling between the spins in the antiferromagnetic and the spins in the ferromagnetic material. Thus in zero external magnetic field H_0, the ground state is illustrated in Fig. 1(a). Note that the ferromagnetic moments alternate in sign as

one moves down the superlattice, and the length of the unit cell is $2(d_1+d_2)$. As a magnetic field is applied, one sees that the configuration in Fig. 1(b) drops below that in Fig. 1(a) in energy, by virtue of the Zeeman energy gained by reorienting the ferromagnetic spins. In appropriate units, one gains the energy $N_{\rm FM}H_0$, where $N_{\rm FM}$ is the number of layers in the ferromagnetic film, and one loses $H_{\rm int}^{(x)}$, a measure of the exchange energy between adjacent sheets of spins at the interface between the two materials. The field required to reorient the ferromagnetic spins is thus $H_{\rm int}^{(x)}/N$, and can be quite small if N is large. Furthermore, the transition field is subject to control through appropriate design of the superlattice structure.

Section II of the present paper explores the field dependence of the ground-state spin configuration for superlattices such as those illustrated in Fig. 1, within which the antiferromagnetic constituent consists of sheets spins each with ferromagnetic alignment. The basis of our treatment is a localized spin model, with nearest-neighbor exchange interactions of appropriate sign in each material. We add uniaxial anisotropy in the antiferromagnetic medium. The superlattices we examine are here all of infinite extent, so we are not concerned with surface phenomena. In Sec. III we examine the nature of the spin waves in the superlattice structure, for the various ground-state spin patterns examined in Sec. II. A subset of the modes are collective excitations of the entire superlattice system, and then we have eigenmodes confined nearly exclusively to one constituent, with character similar to the standing spin-wave resonances of thin films. Section IV presents studies of the magnetic field variation of the microwave and infrared absorption spectrum.

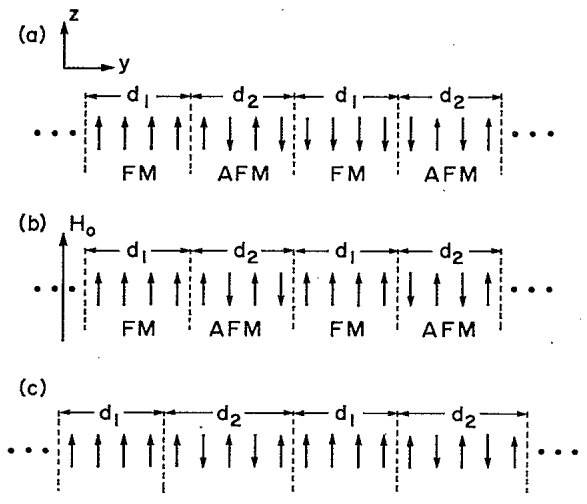

FIG. 1. For the sublattice geometry of interest in the present paper, we show (a) the zero-field ground state when the number of layers in the antiferromagnet is even, (b) possible high-field ground state when an external Zeeman field H_0 is applied, when the number of layers in the antiferromagnet is even, and (c) the zero-field ground state when the number of layers on the antiferromagnet is odd.

II. DETERMINATION OF THE CLASSICAL GROUND STATE OF THE FERROMAGNET-ANTIFERROMAGNETIC SUPERLATTICE: PHASE DIAGRAM AT ZERO TEMPERATURE

As discussed in Sec. I, we study a superlattice that consists of ferromagnetic (FM) films each with $N_{\rm FM}$ layers, and antiferromagnetic (AFM) films each with $N_{\rm AFM}$ layers. Each is a bcc lattice of spins (with the same lattice constant), and the interface is a (100) plane. Each site is occupied by a localized spin S; we assume S to be the same for the FM and AFM, an assumption that has no influence on the basic structure of our results, which in the end are phrased in terms of the relevant exchange and anisotropy field strengths. We have nearest-neighbor exchange interactions of strength $J_{\rm FM}$ within the FM, $J_{\rm AFM}$ within the AFM, and J_I across the interface between the FM and the AFM. Also, within the AFM, we have uniaxial anisotropy, modeled by single-site anisotropy of the form KS_z^2.

Note that for the above geometry, the AFM consists of ferromagnetically aligned sheets of spins, each with spin direction parallel to the (100) plane for the case where the easy axis lies within this plane.[6] In the infinitely extended material, the ground state in zero external magnetic field consists of such ferromagnetic sheets with ferromagnetic alignment alternately up and down.

The ground-state spin arrangement in the superlattice, with zero external field applied, depends on whether the number $N_{\rm AFM}$ of planes in the AFM is even or odd. We have the following two arrangements possible, assuming J_I is ferromagnetic in sign.[7] If N_F is even, then the ground state is that illustrated in Fig. 1(a), and the length of the magnetic unit cell of the superlattice is $2(d_1+d_2)$. Upon adding one more plane of spins to each antiferromagnetic layer, one sees that each ferromagnetic film now has its moment directed in the $+\hat{\mathbf{z}}$ direction, instead of alternating in sign as in Fig. 1(a). Then the magnetic unit cell of the superlattice structure is (d_1+d_2). The ground-state configuration with $N_{\rm AFM}$ odd is illustrated in Fig. 1(c).

We shall begin with a study of the stability of the ground-state spin configurations illustrated in Figs. 1(a) and (c). We do this by adding a magnetic field of strength H_0 parallel to the z axis, then searching for "soft spin waves" in the excitation spectrum of the superlattice. This, then, is an extension to the superlattice geometry of the discussion presented many years ago by Anderson and Callen,[8] for an infinitely extended antiferromagnet. (We believe that some of the results in this paper are not correct, however. We elaborate on this later on.) After we outline the domain of magnetic field within which the simple ground state is stable, we then discuss the magnetic field variation of the ground-state spin configuration at higher fields, to construct a phase diagram of the system (at $T=0$). We then present studies of the spin wave and infrared absorption spectrum of the high-field phases. A brief summary of some of our early results is presented elsewhere.[10]

To proceed, we must choose a set of parameters, and all of our calculations have been carried out for one particu-

lar set. The antiferromagnetic is characterized by the exchange field $H_E = zJ_{\rm AFM}S$ and the anisotropy field[11] $H_A = 2KS$, when K is the anisotropy constant in the single-ion anisotropy term KS_z^2, present for each spin. We choose $H_A/H_E = 0.05$, a value characteristic of MnF_2. We also choose the exchange constant $J_{\rm AFM}$ in the antiferromagnetic to be equal to that in the ferromagnet, and the spins S are also taken equal. We have chosen $J_I = \frac{3}{2}J_{\rm FM} = \frac{3}{2}J_{\rm AFM}$ for the numerical calculations. We have no specific magnetic materials in mind for the ferromagnetic constituent as we make this choice, but we require specific parameters for the numerical analyses. It is useful to partition the remainder of this section into subsections.

A. Instabilities of the low-field ground state

The regime of stability of an assumed ground state configuration of a spin system may be studied through analysis of the spin wave spectrum. If all spin wave excitation energies are positive, one is assured the system resides in a local minimum of the energy in the appropriate parameter space. If the externally applied magnetic field H_0 is varied, and a particular spin wave goes "soft," to acquire negative excitation energy with further increase in field, then the system is unstable. This method, used for stability analyses earlier in other contexts,[8,12] will be employed here to study the stability of the ground state spin configurations displayed in Figs. 1(a) and 1(c), for the two cases $N_{\rm AFM}$ even and $N_{\rm AFM}$ odd.

In the ferromagnetic films, we begin with the equation of motion for the operator $S^+(l)$, with l a particular site in the film. This reads, with Zeeman field H_0 applied parallel to $\hat{z}$,

$$i\frac{dS^+(l)}{dt} = \sum_{\delta} J(l,l+\delta)[S^+(l)S_z(l+\delta) - S^+(l+\delta)S_z(l)] + H_0 S^+(l) \,. \tag{2.1}$$

The sum over δ ranges over nearest neighbors, and in general the exchange coupling J has a dependence on site index l because spins at the interface have neighbors in the antiferromagnet. In the antiferromagnet, we have A and B sublattices in the standard manner, and the effective anisotropy fields for the A and B sublattices are oppositely directed. Thus we have here for the A sublattice spins

$$i\frac{dS^+(l)}{dt} = \sum_{\delta} J(l,l+\delta)[S^+(l)S_z(l+\delta) - S^+(l+\delta)S_z(l)] + H_0 S^+(l) + H_A S^+(l) \,, \tag{2.2}$$

while the sign of H_A is reversed in the equation of motion of the B spins.

We linearize these equations by replacing $S_z(l)$ by $+S$ or $-S$, then look for solutions in which $S^+(l)$ has the time dependence $\exp(-i\Omega t)$. We are then led to an eigenvalue equation for the frequency Ω with the form

$$\Omega S^+(l) - \sum_{l'} M(l,l')S^+(l') = 0 \,, \tag{2.3}$$

where the explicit form of $M(l,l')$ can be constructed from Eqs. (2.1) and (2.2).

We assume that the coordinate system is arranged as illustrated in Fig. 1(a). The z axis is parallel or antiparallel to the magnetization directions of the places in the ground state, and the xz plane is parallel to the interfaces in the superlattice structure. The y axis is thus normal to the interfaces. A given site l has position designated by the three numbers (l_x,l_y,l_z) and we impose periodic boundary conditions in the x and the z directions. We thus have solutions of the Bloch form in the x and z coordinates,

$$S^+(l) = e^{ik_x l_x} e^{ik_z l_z} \mathcal{S}(l_y) \,, \tag{2.4}$$

and then $\mathcal{S}(l_y)$ obeys

$$\Omega \mathcal{S}(l_y) - \sum_{l_y'} m(k_x,k_z;l_y,l_y')\mathcal{S}(l_y') = 0 \,, \tag{2.5}$$

where the dimensionality of the matrix $m(k_x,k_z;l_y,l_y')$ equals that of the number of layers in the unit cell of the superlattice. One has

$$m(k_x,k_z;l_y,l_y') = \sum_{l_x',l_z'} M(l,l')e^{ik_x(l_x'-l)} e^{ik_z(l_z'-l_z)} \,. \tag{2.6}$$

The structure of the matrix $M(k_x k_z;l_y l_y')$ is considered in Appendix A. It is in fact a non-Hermitian matrix, due to the presence of antiferromagnetic films in the superlattice structure. The eigenvectors which emerge as the solution of Eq. (2.5) are thus the right eigenvectors, and they are, in general, distinct from the left eigenvectors.[13] To discuss the response of the superlattice to external perturbations, we require both sets as we shall see.

We then have $2(N_{\rm FM}+N_{\rm AFM})$ eigenvalues $\Omega_\alpha(H_0)$, half of which have positive frequency, and half of which are negative; the excitation energy of a spin wave is $\hbar|\Omega_\alpha(H_0)|$. The stability of the ground state may then be explored by following the spin-wave excitation energies as a function of H_0, and finding the first mode which is driven to zero frequency by application of the field. We find that the soft mode is always the lowest-lying negative frequency wave with $k_x = k_z = 0$.

The value of the critical field $H_0^{(c)}$ differs dramatically in value, depending on whether one has an odd or an even number of layers in the antiferromagnetic constituent. This is illustrated in Fig. 2. In Fig. 2(a), for the case where $N_{\rm AFM} = N_{\rm FM} = N$, and the number of layers in the antiferromagnet is even [see Fig. 1(a)], we see that the critical magnetic field decreases to zero as N is increased. Furthermore, for all values of N considered, the critical field lies far below the spin-flop field of the bulk antiferromagnetic crystal. (The units of magnetic field in Fig. 2 are such that the bulk spin-flop field has the value of unity.) For the case where the number of layers in the antiferromagnet is odd Fig. 2(b), the field required to generate a ground-state instability is always *greater* than the bulk spin-flop field, which is approached asymptotically in the limit $N \to \infty$.

The trends in Fig. 2 may be understood easily by considering the limit of very large N. For the case where $N_{\rm AFM}$ is odd, for large N the field-induced instability is simply the antiferromagnetic spin-flop transition. For N

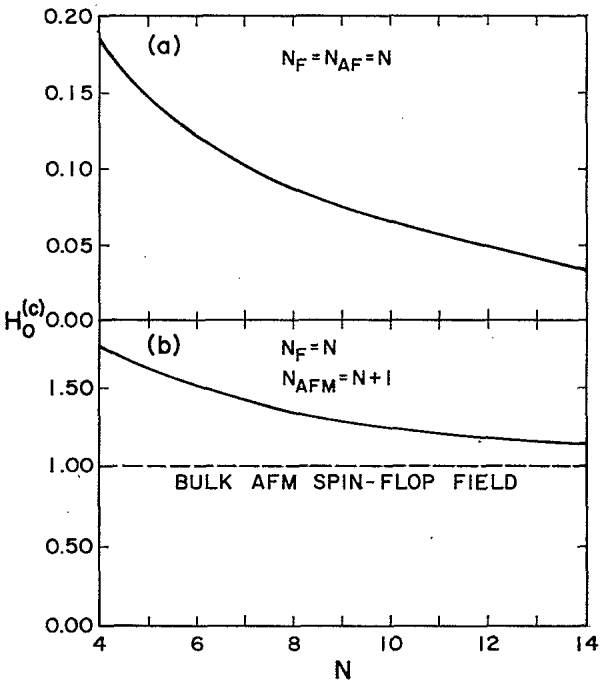

FIG. 2. Critical field for inducing an instability in the ground-state spin configuration, as a function of the number of layers in the films from which the superlattice is fabricated. In (a), we have $N_{FM}=N_{AFM}=N$, with N even, and in (b) we have $N_{FM}=N$, $N_{AFM}=N+1$, again with N even. The units of field are chosen so the bulk spin-flop field on the bulk antiferromagnetic medium equals unity.

large but finite, the field required to induce the spin-flop transition exceeds the bulk spin-flop field by an amount proportional to $1/N$, because the spins near the interface are inhibited by exchange coupling to the ferromagnet, which has spins pinned in the positive z direction by H_0. Thus, for finite N the field required to induce the instability exceeds the bulk spin-flop field, but approaches this value as $N\rightarrow\infty$.

When N_{AFM} is even, a different picture applies. The driving force for the transition is the gain in Zeeman energy in the ferromagnetic film with spins initially down. The energy gain from this source is $2H_0SN$ in the limit of large N. Rotation of the spins in the down-spin ferromagnet applies a 180° twist to the chain of antiferromagnetic spins. The high-field state is then one where a soliton is formed in the middle of the antiferromagnet. The initial spin configurations of the antiferromagnet is $ABAB\ldots ABAB$, and the final configuration (for N_{AFM} large) is $ABAB\ldots$(soliton)$\ldots BABA$. For large N_{AFM}, the field required to induce the transition is then $E_{sol}/2H_0SN$, with E_{sol} the energy required to create the soliton. The critical field thus vanishes as $N\rightarrow\infty$, and can be very small for even modest values of N.

At this point, it is clear that the properties of the superlattice structure are controlled importantly by the detailed arrangement of the atomic planes. Such microscopic details thus influence the macroscopic properties of the material. Suppose, for example, we apply a small static field in the x direction, normal to the Zeeman field H_0 and still parallel to the interfaces. We may calculate χ_{xx}, the static susceptibility that describes the total magnetic moment induced parallel to x by such a field. The field variation of χ_{xx} is displayed in Fig. 3, for two choices of N_{AFM}, one even and one odd. We see a clear divergence as the critical field is approached below. Since the critical fields are rendered very different in value by the addition of only one additional atomic layer of spins in each antiferromagnetic film, there is a very large influence on the macroscopic properties of the sample from a small microscopic structural modification. We also show χ_{xx} for fields a bit above the critical fields for each case; the negative values assumed by this quantity above the critical field insures that the critical field is correctly determined by the soft spin wave criterion, and the ground state is indeed unstable with respect to spin rearrangements. A description of the calculation of χ_{xx} will be provided later in this paper. We now turn to a discussion of the ground-state spin arrangements, when the magnetic field exceeds the critical value.

B. Ground-state spin configuration as a function of external magnetic field

Particularly when the number of spins in the antiferromagnetic film is even, the magnetic field dependence of the ground-state spin configuration on magnetic field is complex.

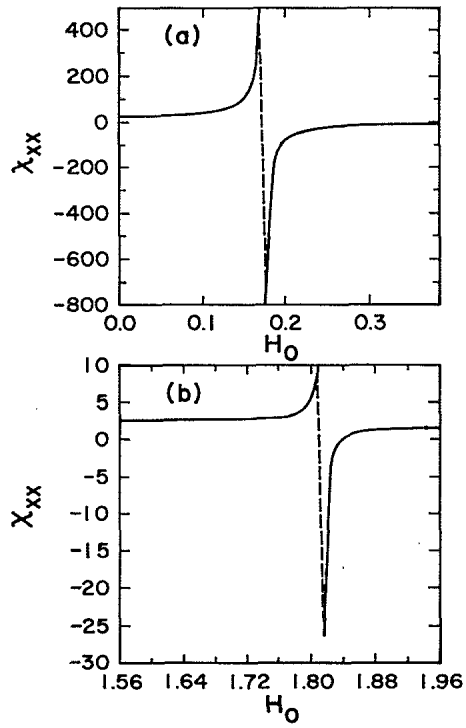

FIG. 3. The transverse static susceptibility χ_{xx} as a function of (normalized) external Zeeman field, for the case (a) of an even number of layers in the antiferromagnetic film ($N_{FM}=N_{AFM}=4$) and (b) an odd number of layers in the antiferromagnetic film ($N_{FM}=4$, $N_{AFM}=5$). In both cases, there is a divergence in χ_{xx} as the first critical field is approached from below.

It is perhaps useful to recall the behavior of the bulk antiferromagnet at $T=0$ before we begin.[8] As H_0 is increased from zero, one first encounters the spin-flop transition at the lower critical field of $(2H_EH_A)^{1/2}$ when $H_E \gg H_A$. The spin-flop transition is a first-order phase transition. As H_0 is increased, the spins on each sublattice rotate into the field H_0, until a second critical field is reached where they are aligned fully with the field, in a configuration of ferromagnetic character. At the point where the spins just align, one has a second-order phase transition. The high-field phase is referred to as the paramagnetic phase.

Quite clearly, for the superlattice, when H_0 is so large that both exchange and anisotropy energy is overwhelmed by the Zeeman energy, we shall realize an analogue of the paramagnetic phase, with all spins aligned fully along H_0. We find two distinctly different phases at intermediate fields for the case where N_{AFM} is even, however. (For N_{AFM} odd, there is only one.) Before we describe these, we comment on the computational method used to construct the magnetic phase diagram.

We begin by supposing the unit cell of the structure is $2(d_1+d_2)$. (This places a constraint on our ability to investigate one point, as noted below.) Then the number of planes of spins in the unit cell is $2(N_{\mathrm{FM}}+N_{\mathrm{AFM}})$. We allow the spins in the ith plane to rotate away from the z axis by the angle θ_i, always confined to the xz plane,[14] so the spin configuration is described by this set of $2(N_{\mathrm{FM}}+N_{\mathrm{AFM}})$ angles. The task is to find the set of angles which minimize the energy of the spin system. We do this by an iterative procedure. We begin with an arbitrarily chosen set of angles. Each spin is then not parallel to the local effective field generated by the spins in neighboring planes, and that associated with the single-site anisotropy energy KS_z^2. We then rotate each spin into its local field, a step which insures that the energy of the system is lowered. We continue until we achieve a configuration in which each spin is aligned with the effective field, and we achieve the set of angles which satisfy the set of energy minimization equations generated by the criterion $\partial(E\{\theta_j\})/\partial\theta_i=0$.

As remarked above, when N_{AFM} is even we find a sequence of two phase transitions, each second order in character, between the zero-field ground state displayed in Fig. 1(a) and the high-field fully aligned state.

The first phase transition is to a configuration we refer to simply as the unsymmetric state. The spins in the down-spin ferromagnet twist away from the $-z$ direction, and this film thus acquires a net magnetic moment parallel to the x direction. This Zeeman-energy-induced twist is resisted by the antiferromagnetic film since, as we see from Fig. 2, we are well below the bulk antiferromagnetic spin-flop field. An exchange torque is exerted on the antiferromagnet, and this is transmitted through to the up-spin ferromagnetic film, with the result that these spins are canted away from the $+z$ direction, by angles *smaller* than those which describe the twist in the down-spin film. For the case $N_{\mathrm{FM}}=N_{\mathrm{AFM}}=4$, and a particular choice of Zeeman field, we show the spin configuration in the unsymmetric phase in Fig. 4(c). Each circle is supposed parallel to the xz plane, and the orientation of the spins in each plane of the unit cell is indicated by an arrow.

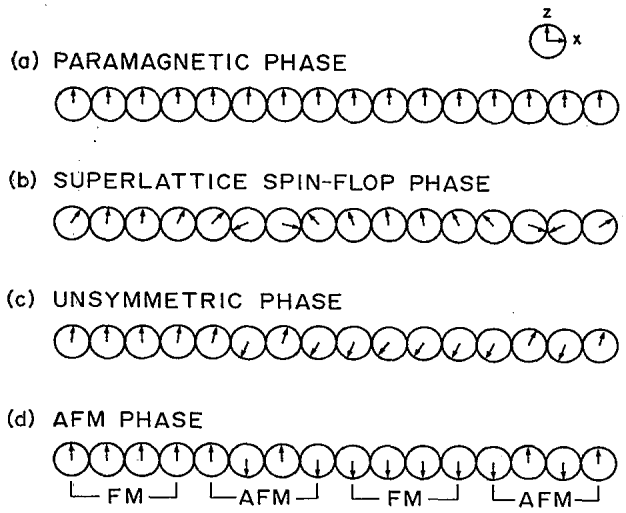

FIG. 4. For $N_{\mathrm{FM}}=N_{\mathrm{AFM}}=4$, we show the spin arrangement in (a) the high-field paramagnetic phase, (b) the superlattice spin-flop phase, (c) the unsymmetric state, and (d) the low-field ground state. Each circle lies in the xz plane, and the arrow indicates the orientation of the spins in a given plane.

Note that each unit cell of the structure has a static transverse moment parallel to the x axis. Our periodicity condition that the unit cell of the superlattice be $2(d_1+d_2)$ prohibits us from inquiring if all the transverse moments of the various unit cells are parallel, thus producing a broken symmetry state with macroscopic moment parallel to x (demagnetizing fields not considered here would render such a state energetically unfavorable), or whether the transverse moments alternate in sign as one moves down the superlattice, producing a unit cell of size $4(d_1+d_2)$. The energy difference between these two configurations would be very tiny for our model Hamiltonian, and it would prove difficult to explore this question.

As the Zeeman field is raised, we encounter a second-order phase transition to a new phase we call the superlattice spin-flop phase. The spin configuration here is illustrated in Fig. 4(b). The spin configuration in one ferromagnetic film is obtained from the second in the unit cell by just a reflection of the spin arrangement through the yz plane. A consequence is that the unit cell now has zero net transverse moment. The structure also has glide-plane symmetry. If the spin arrangement is translated parallel to the y axis by half the length of the unit cell (d_1+d_2), then reflected in the yz plane, we recover the initial state. Note that the bulk antiferromagnetic spin-flop arrangement also has glide-plane symmetry. When we study the spin-wave spectrum of the superlattice spin-flop phase, we shall find the existence of glide-plane symmetry will have a striking effect on the dispersion relation of the modes.

Finally, at high fields, we realize a paramagnetic phase similar in nature to that in the bulk antiferromagnet. The transition from the superlattice spin-flop state to the

paramagnetic state is second order, as in bulk antiferromagnets.

For $N_{FM}=4$, and values of N_{AFM} ranging from 4 to 20, we give the phase diagram of the structure in Fig. 5.

III. SPIN-WAVE EXCITATIONS OF THE SUPERLATTICE STRUCTURE

This section is devoted to an analysis of the spin-wave spectrum of the superlattice structure. We have carried out detailed studies of these elementary excitations as a function of the externally applied Zeeman field H_0, as the field is swept through the phase diagram displayed in Fig. 5.

The formalism we have used in this study is described in Appendix A. In brief, we proceed as follows. If l denotes the site of a particular spin, with the y axis normal to the interfaces in the superlattice structure, the spin at this site is canted away from the $\hat{z}$ axis by the angle θ_{l_y}, with the spin in the xz plane. We erect a new coordinate system $x'y'z'$ at site l, with the z' axis parallel to the spin, and the $x'z'$ plane parallel to the old xz plane. We then obtain linearized equations of motion for the operators $S'_{\pm}(l)=S_{x'}(l)\pm iS_{y'}(l)$, which describe the spin deviations away from the z' axis. Since translational invariance remains in the x and z directions, we may apply periodic boundary conditions in these two coordinates. Thus, we have solutions of the Bloch form, in a more explicit notation,

$$S'_{\pm}(l_x,l_y,l_z)=e^{ik_x l_x}e^{ik_z l_z}\mathcal{S}_{\pm}(l_y)\ . \tag{3.1}$$

The superlattice is also periodic in the y direction, and in the cases of interest the superlattice unit cell consists of $2(N_{FM}+N_{AFM})$ layers of spins. Thus, if l'_y and l_y refer to equivalent planes of spins in different superlattice unit cells, the solutions also have Bloch character in the y direction:

$$\mathcal{S}_{\pm}(l'_y)=e^{ik_\perp(l'_y-l_y)}\mathcal{S}_{\pm}(l_y)\ . \tag{3.2}$$

By using Eqs. (3.1) and (3.2), the problem of calculating the spin-wave spectrum can be reduced to diagonalizing a $4(N_{FM}+N_{AFM})$ dimensional matrix. In general, in the complex canted states, the variable $\mathcal{S}_+(l_y)$ is coupled to $\mathcal{S}_-(l_y)$, so the spin precession is elliptical in nature. For each choice of k_x, k_z, and $k_\perp$ we then have $4(N_{FM}+N_{AFM})$ spin-wave frequencies, half of which are negative and half of which are positive. The excitation energy of a given mode is the absolute value of its frequency $\Omega_\alpha(\mathbf{k})$, where $\mathbf{k}=\hat{x}k_x+\hat{y}k_\perp+\hat{z}k_z$.

We have carried out extensive studies of the superlattice spin-wave spectra, and in the interest of brevity we only summarize the principal features here. In the next section we present studies of the infrared absorption spectrum of the structures. There, only those modes with $k_\perp=0$ and which generate a net transverse dipole moment contribute, as we shall see.

We first begin with the spin-wave spectrum of the low-field ground states illustrated in Figs. 1(a) and 1(c). In this state, the spin waves have the character of standing-wave resonances in the constituent films. From the point of view of a given ferromagnetic film, the surrounding antiferromagnet regions act as a source of pinning, because the resonance frequencies of the ferromagnetic and antiferromagnetic media differ substantially. A disturbance in one medium thus does not propagate through the neighboring film, with the consequence that the spin waves have the character of standing-wave resonances of the individual constituents.

There is, of course, a disturbance which decays to zero in an exponential fashion into the neighboring constituents, as one of the modes discussed above is excited. Generally speaking, we find the amplitude of the spin motion in the first layer of spins in the neighboring films can be appreciable, and this then decays rapidly as one penetrates further. The exponential "tails" which extend into neighboring films lead to interaction between modes localized in nearby films of similar character (say between modes localized in adjacent ferromagnetic films), and this leads to dispersion in the superlattice eigenfrequencies, as the component of wave vector $k_\perp$ normal to the interfaces is varied.

The magnitude of this dispersion is sensitive to whether the number of layers N_{AFM} in the antiferromagnetic films is even of odd. We illustrate this in Figs. 6(a) and 6(b). In Fig. 6(a), we show this dispersion in $k_\perp$ of the three lowest

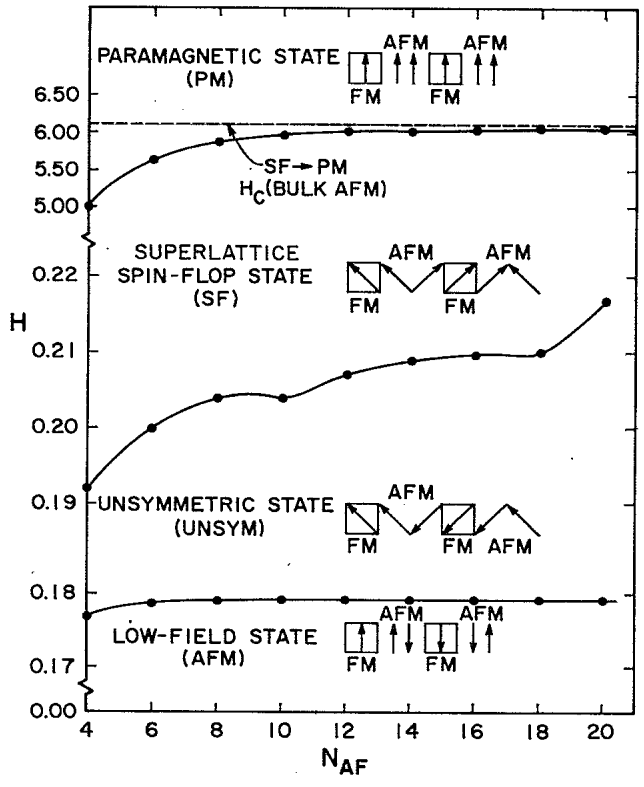

FIG. 5. For the case $N_{FM}=4$, and various values of N_{AFM}, we plot the critical fields required for the various phase changes discussed in the main text. The inset gives the magnetic fields at which phase transitions occur in the bulk antiferromagnetic material. There is no hysteresis in the superlattice transitions as there is at the bulk antiferromagnetic phase transition, since the superlattice phase transitions are second order in character.

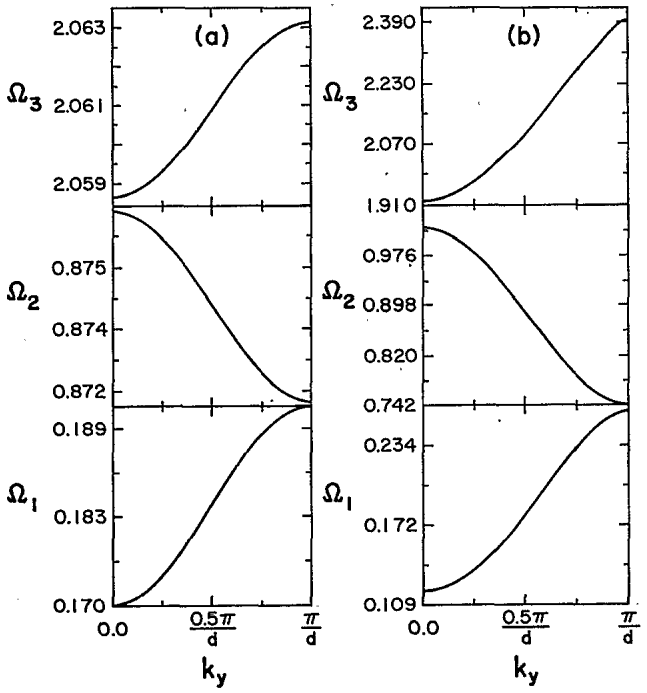

FIG. 6. For $k_x=k_z=0$, we show the dispersion relations of the three lowest frequency spin-wave branches of two superlattice structures. The wave vector $k_\perp$ normal to the interfaces ranges through the superlattice Brillouin zone. The calculations assume the external field $H_0=0$. The two cases considered are (a) $N_{FM}=4$, $N_{AFM}=4$, where the ground state is that illustrated in Fig. 1(a) and (b) $N_{FM}=4$, $N_{AFM}=5$ where the ground state is that illustrated in Fig. 1(c). The units of frequency are such that in the bulk antiferromagnet, the zero-field antiferromagnetic resonance frequency is unity.

frequency spin-wave branches for $k_x=k_z=0$, for the case where $N_{FM}=N_{AFM}=4$. All three modes show very little dispersion; the choice of frequency scale is such that the small amount of dispersion present is magnified. The situation differs substantially when we examine the case where $N_{FM}=4$, but now $N_{AFM}=5$. We see substantial dispersion here, for all three branches. To appreciate the origin of the difference, consider a mode localized in an up-spin ferromagnetic film. When $N_{AFM}=4$, two adjacent up-spin ferromagnetic films are separated by two intervening antiferromagnetic films, with a down-spin ferromagnetic film between them. There are thus twelve layers of nonresonant spins between adjacent resonant films. Thus, modes localized in adjacent up-spin ferromagnetic films are separated by so many layers of nonresonant spins that interaction between them is very modest. On the other hand, when $N_{AFM}=5$, two adjacent up-spin ferromagnets are separated by only five intervening nonresonant layers, and cross-coupling effects can be substantially larger.

As the Zeeman field H_0 is raised, to approach the value required to induce a transition to the unsymmetric state, the mode with lowest excitation energy (a negative frequency mode) approaches zero frequency, and plays the role of the "soft mode" of the upcoming second-order phase transition. At fields well below the phase transition, the mode that evolves into the soft mode is localized in the down-spin ferromagnet. We shall encounter this mode again in Sec. IV, when we discuss the infrared absorption spectrum of the superlattice structure.

In Fig. 7(a) we show the two lowest positive frequency spin-wave branches, again for propagation normal to the interface, for a magnetic field H_0 sufficiently large to drive the system into the unsymmetric state. The calculations are for the case $N_{FM}=N_{AFM}=4$. The lowest branch has a frequency which vanishes linearly with wave vector, as $k_\perp \to 0$. This is in fact the Goldstone mode of the system, which has vanishing frequency as $k_\perp \to 0$ by virtue of the fact that one may continuously rotate the spins about the z axis, without affecting the energy of the system. (The existence of this symmetry operation depends on the fact that we have ignored dipolar interactions in the present treatment.) It follows that this low-frequency branch is in fact a collective mode of the superlattice structure as a whole, rather than an eigenmode localized in the near vicinity of one constituent. The second branch in Fig. 7(a), labelled Ω_2, is also a collective mode of the structure. As the Zeeman field is raised to a value close to that required to induce a transition to the super-

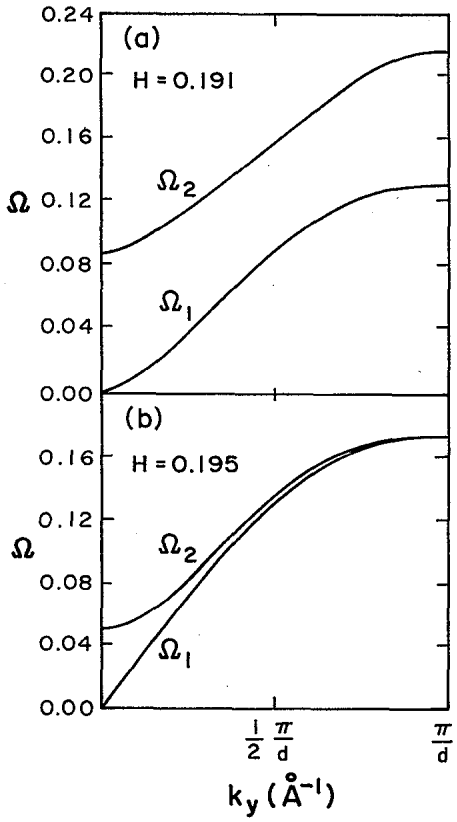

FIG. 7. The lowest two positive frequency spin-wave branches for an external magnetic field H_0 which places the structure in (a) the unsymmetric state and (b) the superlattice spin-flop state. We have chosen $N_{FM}=N_{AFM}=4$ for these calculations.

lattice spin-flop state, the frequency of the $k_\perp=0$ second branch spin decreases to zero; this is then the soft mode associated with the second-order phase transition from the unsymmetric to the superlattice spin-flop state.

In Fig. 7(b), we show the lowest two positive frequency spin-wave branches for a field just above that required to drive the system into the superlattice spin-flop state. The Goldstone mode remains, as symmetry requires, and we see that the $k_\perp=0$ mode associated with the second branch has stiffened somewhat. A new feature is the absence of a gap between the two branches at the Brillouin zone boundary; the two lowest branches merge, and we have a twofold degeneracy at this point. In fact, *all* the spin-wave branches are twofold degenerate at the Brillouin zone boundary, in the superlattice spin-flop state.

At higher fields, the behavior of the spin-wave branches at the Brillouin-zone boundary is illustrated more clearly. In Fig. 8, we show the two lowest positive-frequency spin branches at higher fields. We see the twofold degeneracy again, and note that as one moves away from the zone boundary, there is a linear slope in the dispersion curves. This behavior reminds one of the behavior of electron energy bands in graphite along the face of the crystal Brillouin zone normal to the c axis. One again has a twofold degeneracy in the branch, and there is a linear slope as one moves away from this zone face. From group theoretic arguments, one sees that in graphite, the presence of glide-plane symmetry[15] is responsible for this unusual behavior. Precisely the same argument applies to the spin waves in the superlattice explored here, for Zeeman fields H_0 which place it in the superlattice spin-flop state. As noted earlier, this spin arrangement has a glide plane in its symmetry group. The unsymmetric phase present at lower fields lacks the glide plane, and a consequence is that there are gaps between the various spin-wave branches at the zone boundary, and the dispersion curves exhibit the standard quadratic variation with wave vector, in the near vicinity of the zone boundary. This is illustrated in Fig. 7(a).

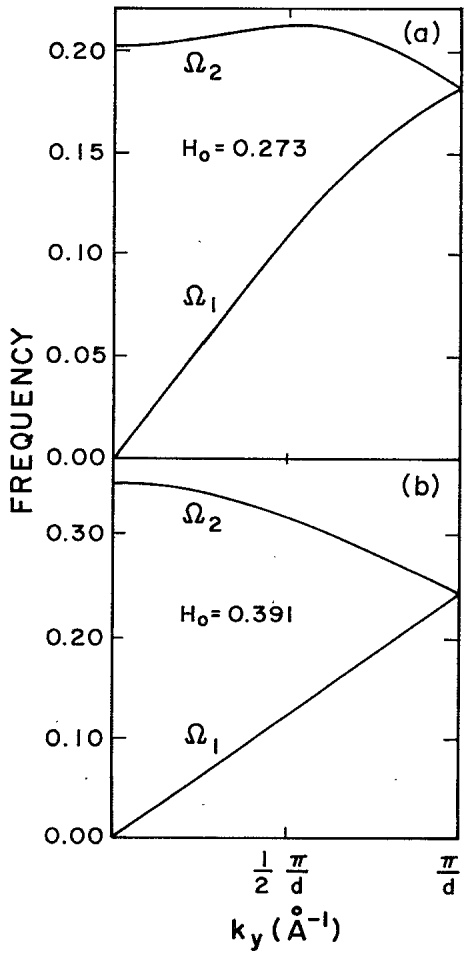

FIG. 8. The lowest two positive frequency spin-wave branches for an external magnetic field H_0 which places the structure in the superlattice spin-flop state. Again the calculations are for $N_{FM}=N_{AFM}=4$.

We pause in our discussion of superlattices to comment on the results obtained in the classic papers by Anderson and Callen[8] and Wang and Callen[9] which discuss spin-wave dispersion relations in the spin-flop phase of the infinitely extended uniaxial antiferromagnet. In their full theory, these authors consider in plane anisotropy described by an anisotropy constant K_2, as well as uniaxial anisotropy described by K_1. In the spin-flop state and with $K_2=0$, these authors find a finite gap in the spin-wave spectrum at zero wave vector, in violation of the Goldstone theorem. Indeed, they comment explicitly that inclusion of K_2, which destroys the continuous Goldstone symmetry, leads to no qualitative change in the spin-wave spectrum. Furthermore, their dispersion relation yields a gap and quadratic dispersion curves near the zone boundary, although the bulk spin-flop state also has glide-plane symmetry. Through a scheme described only briefly in their paper, these authors incorporate the influence of zero-point fluctuations on the spin-wave spectrum; this introduces corrections in the dispersion relation the order of $1/S$. If these zero-point corrections are omitted from their expressions, then one obtains spin-wave dispersion relations consistent with the requirements of Goldstone and glide-plane symmetry arguments. Since these requirements are group theoretic in origin, they apply also to a quantum system with zero-point fluctuations. It is our view that the procedure used by these authors to generate zero-point fluctuation corrections to the spin-wave dispersion relations is evidently in error.

This summarizes our studies of spin waves in the various phases of the superlattice structure. We see that each second-order phase transition has a "soft mode" associated with it, and in the high-field low-symmetry phases the low-frequency branches have the character of collective excitations of the entire structure, as opposed to waves approximately localized to one constituent of the structure.

IV. INFRARED ABSORPTION SPECTRUM OF THE SUPERLATTICE

One means of obtaining information about the spin configuration of the superlattice is the study of the microwave or near-infrared absorption spectrum. In Appendix B, we describe the method of calculating the absorption spectrum, and in this section we present the results of

our study of the model superlattices explored earlier in the paper.

In Fig. 9, we show the calculated absorption spectrum for the low-field ground-state spin configuration displayed in Figs. 1(a) and 1(c). The units of frequency are such that the zero-field bulk antiferromagnetic resonance frequency is unity. Figures 9(a)—9(c) show calculations for the case $N_{FM}=N_{AFM}=4$, while calculations displayed in Figs. 9(d)—9(f) show calculations for the case $N_{FM}=4$, $N_{AFM}=5$. From Fig. 2(a), we see that when $N_{FM}=N_{AFM}=4$, the low-field ground state becomes unstable for a reduced field $H_0\cong 0.18$, while when $N_{AFM}=5$, it remains stable up to a field $H_0\cong 1.8$, substantially larger than the bulk spin-flop field of 1.0.

In Fig. 9(a), we show the absorption spectrum for the case where $N_{FM}=N_{AFM}=4.0$, and the external Zeeman field $H_0=0$. The high-frequency feature is the absorption associated with the lowest frequency mode localized in the antiferromagnetic film. As remarked in Sec. III, the surrounding ferromagnetic films act to partially "pin" the spins near the interface, so the spin-deviation associated with this mode is rather similar to the ground-state wave function of a quantum mechanical particle in a one-dimensional, deep but finite potential well. The spins in the ferromagnetic films immediately adjacent to the antiferromagnets participate appreciably in the mode; this is a spin analogue to leakage of the quantum mechanical wave function into the classically forbidden regions. The mode is shifted above the bulk antiferromagnetic resonance frequency of 1.0 by the pinning, which enhances the exchange contribution to the excitation energy of this mode. We see a weak feature at higher frequency that is the "first excited state" of the antiferromagnetic film.

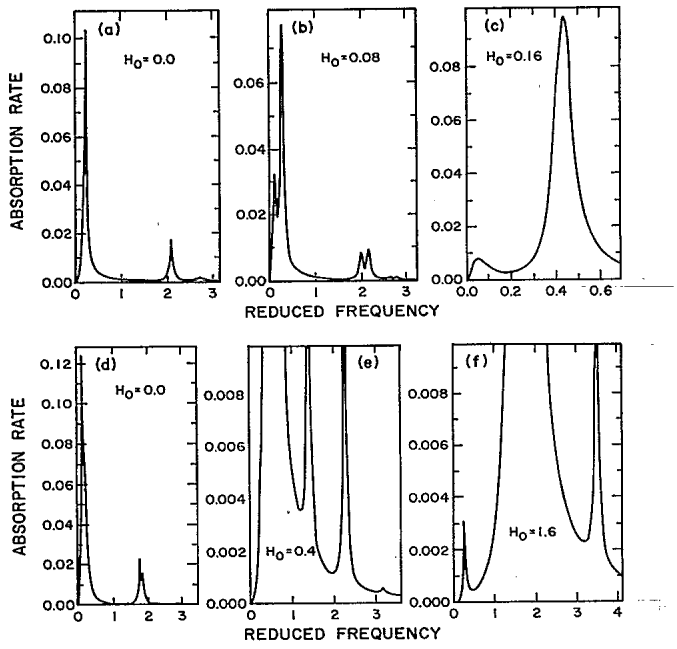

FIG. 9. The infrared absorption spectrum, in arbitrary units, for two model superlattices and various magnetic fields. In (a)—(c), we have calculations for the case $N_{FM}=N_{AFM}=4$, while in (d)—(f), we present calculations for the case $N_{FM}=4$, $N_{AFM}=5$. The units of frequency are such that in the bulk antiferromagnetic material, the zero-field antiferromagnetic resonance frequency is unity. The magnetic field H_0 is measured in units of $(2H_EH_A)^{1/2}$.

The strong low-frequency feature is a mode localized in the ferromagnetic films. In zero external field, this has finite frequency by virtue of the pinning provided by the neighboring antiferromagnetic films. There are modes localized in the up-spin ferromagnetic films, and modes localized in the down-spin films, and in zero external field these involve opposite senses of spin precession. Both contribute to the calculated absorption spectrum since, as discussed in Appendix B we assume the driving field to be linearly polarized along the $\hat{\mathbf{x}}$ direction.

Figure 9(b) shows the influence of a weak Zeeman field. The modes localized in the antiferromagnetic films split, in a manner familiar from antiferromagnetic resonance studies of bulk materials. The feature with origin in the ferromagnetic film splits also, since application of the Zeeman field renders the two ferromagnetic films inequivalent. The mode associated with the down-spin film is the one which softens, and as H_0 increases, this mode becomes the "soft mode" associated with the second-order magnetic-field-induced phase transition to the unsymmetric state. In Fig. 9(c), we show the absorption spectrum calculated for a field just a bit below that required to drive the low-field ground state unstable. Note that the frequency scale in Fig. 9(c) differs from that in Figs. 9(a) and 9(b). The critical fields displayed earlier in Fig. 2 are calculated by finding the field at which the mode just described becomes "soft." The energy minimization calculations place the phase transition at the same field, as expected for a second-order phase transition.

Figure 9(d) shows the zero-field absorption spectrum for the case $N_{AFM}=5$, where in the low ground state, all spins in the ferromagnetic film are directed upward [Fig. 1(c)]. The spectrum in Fig. 9(d) is qualitatively similar to that in Fig. 9(a) except that in zero external field, the resonance associated with the antiferromagnetic film suffers a small splitting. This splitting is produced by the exchange coupling between the antiferromagnetic and the neighboring ferromagnetic films, both of which are "up," and exert a net effective magnetic field in the antiferromagnet through the exchange coupling across the interface.

As the field is raised, the low frequency partner of the antiferromagnetic resonance doublet is driven downward and that associated and the ferromagnetic film stiffens, as one sees in Fig. 9(e). With further increase in field there is a level crossing and strong mixing between the two modes, and finally with still further increase in field, a soft mode emerges on the low-frequency side of the doublet. Fig. 9(f) shows the absorption spectrum calculated for a field just below that required to drive the low-field ground state unstable.

From a very qualitative point of view, the picture just described bears a resemblance to the soft modes associated with the ferroelectric phase transition. Here temperature is the parameter which drives the optical phonon soft as it decreases. Close to the phase transition, the optical mode softens to the point where it admixes strongly with acoustical phonons, and in the end the soft mode is an ad-

mixture of acoustical and optical modes.

We have also carried out calculations of the absorption spectrum of the high-field, low-symmetry states. Figure 10(a) shows the spectrum of the unsymmetric state, at a value of the Zeeman field H_0 just above the transition to the unsymmetric state. The absorption spectrum is rich; the prominent low-frequency feature is the mode labeled Ω_2 in Fig. 7(a). [In Fig. 7(a), the calculations are carried out for a larger value of the magnetic field.] As remarked earlier, this mode, like the very low-frequency Goldstone mode, is a collective mode of the whole superlattice structure. As the magnetic field H_0 is increased, to approach the field required to induce a transition to the superlattice spin-flop state, this mode softens, and the higher-frequency absorption lines progressively weaken in oscillator strength. The Ω_2 mode is the soft mode of the phase transition from the unsymmetric to the superlattice spin-flop state. In Fig. 10(b), we show the spectrum at a field slightly below that associated with the transition.

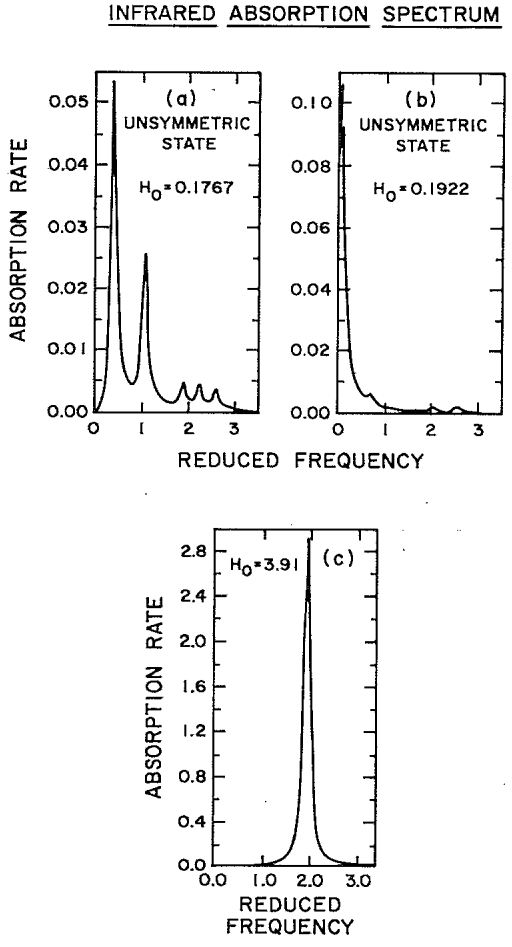

FIG. 10. For $N_{FM}=N_{AFM}=4$, we show the infrared absorption spectrum for several fields when the system is in the low-symmetry ground states. In (a), the Zeeman field is out just a bit above the transition from the low-field ground state to the unsymmetric state; in (b) it lies just a bit below that required to induce the superlattice spin flop state; and in (c) it is sufficiently large for the system to be within the superlattice spin-flop state. The units of field and frequency are the same as those used in Fig. 9.

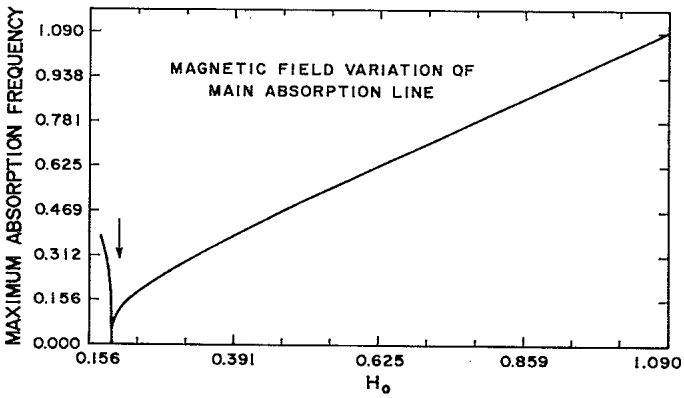

FIG. 11. For $N_{FM}=N_{AFM}=4$, we show the magnetic field variation of the dominant feature in the absorption spectrum, as the Zeeman field is swept through the unsymmetric state into the superlattice spin-flop state. The units are the same as those in Fig. 9.

In the superlattice spin-flop state, we find a single feature in the absorption spectrum. For a particular choice of field, this spectrum is illustrated in Fig. 10(c). This feature has a frequency which increases with H_0 in a linear manner. In Fig. 11, we show the field dependence of this dominant feature in the absorption spectrum, as the magnetic field is swept through the phase transition from the unsymmetric to the superlattice spin-flop state, and then to values well into the superlattice spin-flop state.

V. CONCLUDING REMARKS

This paper has been devoted to a theoretical study of a model of a superlattice fabricated from alternating layers of ferromagnetic and antiferromagnetic materials. We find rich behavior; macroscopic properties of the resulting material, such as the phase diagram and the optical absorption spectrum, are influenced strongly by microscopic details of the underlying superlattice.

Our work has confined its attention to model materials described by the localized spin picture of magnetism. It is our view that this phenomenology can describe, qualitatively, the energy changes associated with spin rearrangements in media where itinerant electrons carry the magnetic moment. As a consequence, we expect rich behavior in superlattices formed by such materials as well.

At the time of this writing, no systems have been fabricated which serve as a test of the predictions set forth here. There is, however, literature on multilayer structures formed from alternating layers of ferromagnetic and antiferromagnetic materials. Examples are Co-Cr superlattices (the spin density wave in bulk Cr has a period which differs from the lattice constant by only a few percent; we expect that in very thin, high quality Co films, boundary effects will force the system to become commensurate) and superlattices formed from MnFe and permalloy. In the examples studied so far, the individual layers are hundreds of layers thick. Also, we expect the quality of the interfaces in the materials realized so far is very poor. We plan further studies of other superlattice

geometries in which very different behavior may be expected.

ACKNOWLEDGMENT

This research is supported by the U.S. Army Research Office (Durham, NC), through Grant No. PO426620.

APPENDIX A: FORMALISM EMPLOYED TO CALCULATE THE SPIN-WAVE SPECTRUM OF THE SUPERLATTICE STRUCTURE

In the main text of the paper, we discussed the spin-wave spectrum of the superlattice structure, with emphasis on the complex canted states which exist above the lowest critical field which drives the zero-field ground state unstable. In this Appendix, we discuss the formalism upon which these calculations were based.

The basic Hamiltonian consists of exchange, Zeeman and uniaxial anisotropy terms which we write

$$H=-\tfrac{1}{2}\sum_{l,\delta}J(l,l+\delta)\mathbf{S}(l)\cdot\mathbf{S}(l+\delta) -H_0\sum_l S_z(l)-K\sum_{l_{\rm AFM}}S_z^2(l_{\rm AFM})\ , \tag{A1}$$

where the uniaxial anisotropy acts only within the antiferromagnet. We assume S is sufficiently large that the spin system can be treated classically throughout.

In general, the ground state is complex in nature, with spins in each atomic sheet canted away from the $\hat{\mathbf{z}}$ axis by an angle we call θ_{l_y}. Our energy minimization calculation provides us with the set of angles θ_{l_y} associated with each external field H_0. Recall that in our geometry, the interfaces between adjacent films in the superlattice structure are all parallel to the xz plane, the Zeeman field is applied parallel to $+\hat{\mathbf{z}}$ [Eq. (A1)], and thus the y axis is normal to the interface between adjacent films. Within the sheet l_y, all spins lie in the xz plane. We erect an axis $\hat{\mathbf{z}}'$ in this plane, with $\hat{\mathbf{z}}'$ aligned along the spin direction. The new coordinate system is obtained by a rotation through the angle θ_{l_y} about the $\hat{\mathbf{y}}$ axis.

We erect such a new coordinate system for each sheet of spins, and we express each term of the Hamiltonian in terms of the spin components $S'_z(l)$, $S'_+(l)$, and $S'_-(l)$ as measured in the canted coordinate system. Thus, when considering exchange couplings between spins in adjacent sheets, we have

$$\begin{aligned}\mathbf{S}(l)\cdot\mathbf{S}(l')=&\tfrac{1}{4}[A(l_y,l'_y)-1][S'_+(l)S'_+(l')+S'_-(l)S'_-(l')]\\&+\tfrac{1}{4}[A(l_y,l'_y)+1][S'_+(l)S'_-(l')+S'_-(l)S'_+(l')]+A(l_y,l'_y)S'_z(l)S'_z(l')\\&+\tfrac{1}{2}B(l_y,l'_y)\{[S'_+(l)+S'_-(l)]S'_z(l')-S'_z(l)[S'_+(l')+S'_-(l')]\}\ ,\end{aligned} \tag{A2}$$

where

$$A(l_y,l'_y)=\cos(\theta_{l_y})\cos(\theta_{l'_y})+\sin(\theta_{l_y})\sin(\theta_{l'_y})\ ,$$

and (A3)

$$B(l_y,l'_y)=\cos(\theta_{l_y})\sin(\theta_{l'_y})-\sin(\theta_{l_y})\cos(\theta_{l'_y})\ .$$

Also, we have the identity

$$S_z^2(l_{\rm AFM})=\cos^2(\theta_{l_y})S'_z(l_{\rm AFM})^2+\tfrac{1}{2}\cos(\theta_{l_y})\sin(\theta_{l_y})S'_z(l)[S'_+(l)+S'_-(l)]+\tfrac{1}{4}\sin^2(\theta_{l_y})[S'_+(l)+S'_-(l)]^2\ . \tag{A4}$$

We used the Hamiltonian transformed in the above manner to generate equations of motion for the operators $S'_+(l)$ and $S'_-(l)$, which are the spin-deviation operators in the canted coordinate system. We linearize the resulting equations of motion by replacing $S'_z(l)$ by S everywhere. The terms in the Hamiltonian proportional to $S'_z(l')[S'_+(l)+S'_-(l)]$ lead to terms in the linearized equations of motion independent of either $S'_+(l)$ or $S'_-(l)$. These terms vanish identically if the angles θ_{l_y} are chosen to be those which minimize the energy of the system. With the θ_{l_y} so chosen, in effect each spin is aligned parallel to the effective local molecular field which acts at its lattice site, and no torque acts on the spin when it is aligned along the $\hat{\mathbf{z}}'$ axis.

When we examine the linearized equations of motion for solutions proportional to $\exp(-i\Omega t)$, we have

$$\begin{aligned}\Omega S'_+(l)=&S\sum_\delta J(l,l+\delta)\{A(l_y,l_y+\delta_y)S'_+(l)-\tfrac{1}{2}[1+A(l_y,l_y+\delta_y)]S'_+(l+\delta)+\tfrac{1}{2}[1-A(l_y,l_y+\delta_y)]S'_-(l+\delta)\}\\&+H_0\cos(\theta_{l_y})S'_+(l)+KS(3\cos^2\theta_{l_y}-1)S'_+(l)-KS\sin^2\theta_{l_y}S'_-(l)\ ,\end{aligned} \tag{A5}$$

and

$$\begin{aligned}\Omega S'_-(l)=&-S\sum_\delta J(l,l+\delta)\{A(l_y,l_y+\delta_y)S'_-(l)+\tfrac{1}{2}[1+A(l_y,l_y+\delta_y)]S'_-(l+\delta)-\tfrac{1}{2}[1-A(l_y,l_y+\delta_y)]S'_+(l+\delta)\}\\&-H_0\cos(\theta_{l_y})S'_-(l)-KS(3\cos^2\theta_{l_y}-1)S'_-(l)+KS\sin^2\theta_{l_y}S'_+(l)\ .\end{aligned} \tag{A6}$$

We now invoke Bloch's theorem. We may do this in two steps. First, we have translational symmetry in the two directions parallel to the interfaces, the x and the z direction. Thus, noting that a given site is labeled by the three integers l_x, l_y, and l_z, we have

$$S'(l)=e^{ik_x l_x}e^{ik_z l_z}\mathcal{S}_{\pm}(l_y)\ . \tag{A7}$$

We assume k_x and k_z are fixed by periodic boundary conditions on the xz plane.

The superlattice is also periodic in the y direction. For all cases considered here, the unit cell consists of $2(N_{\rm FM}+N_{\rm AFM})$ layers of spins, where $N_{\rm FM}$ and $N_{\rm AFM}$ is the number of sheets of spins in the ferromagnet and in the antiferromagnet, respectively. We may thus apply Bloch's theorem in the y direction as follows. We choose a particular unit cell of the superlattice as a reference cell, and let l_y refer to a sheet of spins of this cell. Then l_y ranges from 1 to 2 $(N_{\rm FM}+N_{\rm AFM})$. For a given value of l_y, let l_y' refer to the equivalent spin sheet in some other unit cell, i.e., if a_0 is the spacing between adjacent sheets, and $d=2(N_{\rm FM}+N_{\rm AFM})a_0$ is the length of the superlattice unit cell, then $l_y'=l_y+md$, where m is an integer. We may then write

$$\mathcal{S}_{\pm}(l_y')=e^{ik_\perp(l_y'-l_y)}\mathcal{S}_{\pm}(l_y)\ , \tag{A8}$$

where $k_\perp$ lies in the first Brillouin zone of the superlattice structure. We have $-\pi/d\le k_\perp\le+\pi/d$, again with d the dimension of the superlattice unit cell.

If $N=2$ $(N_{\rm FM}+N_{\rm AFM})$ is the number of spin sheets in each superlattice unit cell, then the problem reduces to the diagonalization of a $2N\times 2N$ matrix $\underline{M}(l_y,l_y')$ whose elements, of course, depend on k_x, k_z, and $k_\perp$. For each value of l_y in the reference unit cell, we have two dynamical variables, $\mathcal{S}_+(l_y)$ and $\mathcal{S}_-(l_y)$. Thus, for each choice of the wave vector $\mathbf{k}=\hat{\mathbf{x}}k_x+\hat{\mathbf{y}}k_\perp+\hat{\mathbf{z}}k$, we have $2N$ eigenfrequencies $\Omega_\alpha(\mathbf{k})$. For the low-field ground state illustrated in Fig. 1(a), incidentally, where all angles θ_{l_y} are either 0 or π, the problem decomposes into that of diagonalizing two matrices, each an $N\times N$ matrix.

We introduce a $2N$-dimensional column vector $\underline{S}$, defined as

$$\underline{S}=\begin{bmatrix}\mathcal{S}_+(l_1)\\ \mathcal{S}_+(l_2)\\ \vdots\\ \mathcal{S}_+(l_N)\\ \\ \mathcal{S}_-(l_1)\\ \mathcal{S}_-(l_2)\\ \vdots\\ \mathcal{S}_-(l_N)\end{bmatrix}\ , \tag{A9}$$

so our eigenvalue problem may be written as

$$\sum_{j=1}^{2N}M_{ij}S_j^{(\alpha)}=\Omega_\alpha S_i\ . \tag{A10}$$

From the equations of motion outlined earlier, one may construct the matrix M_{ij}. Its detailed form is of little general interest, but we comment on its general structure.

One may express M in terms of two $N\times N$ matrices, each of which is Hermitian. We call these M_1 and M_2, and we have

$$\underline{M}=\begin{bmatrix}\underline{M}_1 & \underline{M}_2\\ -\underline{M}_2 & -\underline{M}_1\end{bmatrix} \tag{A11}$$

so the matrix $\underline{M}$ is in fact non-Hermitian.

In this case, the eigenvector defined in Eq. (A10) is a right eigenvector, henceforth denoted by $S_j^{(R\alpha)}$, and the right eigenvectors are distinct from the left eigenvectors, which satisfy

$$\sum_j S_j^{(L\alpha)}M_{ji}=\Omega_\alpha S_i^{(L\alpha)}\ , \tag{A12}$$

with Ω_α the same eigenvalue as that which appears in Eq. (A10). The completeness relation, for a given wave vector $\mathbf{k}$, is expressed in terms of both sets of eigenvectors as follows:

$$\sum_{\alpha=1}^{2N}S_i^{(L\alpha)}S_j^{(R_\alpha)}=\delta_{ij}\ . \tag{A13}$$

To study the spin-wave spectrum of the superlattice, we need not be concerned with the nature of the eigenvectors. However, to discuss the response of the superlattice to an externally imposed field, one needs to employ both sets, as one sees from Sec. IV of the main text. An excellent discussion of the eigenvalues spectrum and eigenvectors of non-Hermitian matrices is given in the classic text of Friedman.[13]

APPENDIX B: RESPONSE OF THE SUPERLATTICE TO AN EXTERNAL MAGNETIC FIELD

In this appendix, we discuss the details of the calculation of the response of the superlattice to an externally applied, time-dependent magnetic field. For definiteness, we apply the external field parallel to the x axis, and allow it to have an arbitrary spatial variation. Thus, at lattice site l, the spin is driven by the field

$$\mathbf{h}(l,t)=h_x(l)\cos(\Omega t)\hat{\mathbf{x}}=\tfrac{1}{2}h_x(l)(e^{i\Omega t}+e^{-i\Omega t})\hat{\mathbf{x}}\ , \tag{B1}$$

so this introduces into the Hamiltonian the interaction term

$$V=-\tfrac{1}{2}\sum_l h_x(l)\cos(\Omega t)[S_+(l,t)+S_-(l,t)]\ . \tag{B2}$$

We shall first discuss the response of the system when it resides in the low-field ground state illustrated in Fig. 1(a) or Fig. 1(b). The same principles may be used to extend the analysis to the various canted spin configurations. In the interest of brevity, we comment only briefly on this extension.

In the standard manner, we obtain equations of motion for the operators $S_\pm(l,t)$, and linearize these by replacing $S_z(l)$ by $+S$ or $-S$, whichever is appropriate. In what follows, $S(l)$ will assume the value $+S$ for up spins, and $-S$ for down spins. We shall write, for the response,

$$S_\pm(l,t)=S_\pm^{(1)}(l)e^{i\Omega t}+S_\pm^{(2)}(l)e^{-i\Omega t}\ . \tag{B3}$$

We then find

$$\pm\Omega S_{\pm}^{(1)}(l)-\sum_{l'}M(l,l')S_{\pm}^{(1)}(l')=-\tfrac{1}{2}S(l)h_x(l) \tag{B4a}$$

and

$$\mp\Omega S_{\pm}^{(2)}(l)-\sum_{l'}M(l,l')S_{\pm}^{(2)}(l')=-\tfrac{1}{2}S(l)h_x(l)\ , \tag{B4b}$$

where the matrix $M(l,l')$ is identical to that which enters the analysis of the spin-wave spectrum. In the low-field ground state, $S_+(l)$ does not couple to $S_-(l)$; the matrix $M(l,l')$ is readily constructed from Eq. (A5) through appropriate selection of the angles θ_{l_y}.

The inhomogeneous equations displayed as Eqs. (B4) may be solved formally through construction of an appropriate Green's function. We discuss the construction of this function, then use it to solve Eqs. (B4). The matrix $M(l,l')$ which enters Eqs. (B4) is non-Hermitian, by virtue of the antiferromagnetic regions of the superlattice. We first begin with brief comments on the mathematical structure of the eigenvalue problem associated with non-Hermitian matrix operators.[13]

Non-Hermitian matrices have left eigenvectors which are distinct from right eigenvectors. If $A(i,j)$ is such a matrix, the right eigenvector $e_R^{(\alpha)}(i)$ associated with the eigenvalue λ_α satisfies

$$\sum_j A(i,j)e_R^{(\alpha)}(j)=\lambda_\alpha e_R^{\alpha}(i)\ , \tag{B5}$$

while the left eigenvector $e_L^{(\alpha)}(i)$ satisfies

$$\sum_j [e_L^{(\alpha)}(j)]^* A(j,i)=\lambda_\alpha [e_L^{\alpha}(i)]^*\ , \tag{B6}$$

where the eigenvalue which enters Eq. (B6) is the same as that which enters Eq. (B5). The completeness relation assumes the form

$$\sum_\alpha [e_L^{(\alpha)}(i)]^* e_R^{(\alpha)}(j)=\delta_{ij}\ , \tag{B7}$$

and the orthonormality condition reads

$$\sum_i [e_L^{(\alpha)}(i)]^* e_R^{(\alpha')}(i)=\delta_{\alpha\alpha'}\ . \tag{B8}$$

The Green's functions which may be used to solve Eqs. (B4) may be written as

$$G_{\pm}(l,l')=\sum_\alpha \frac{[e_L^{(\alpha)}(l')]^* e_R^{(\alpha)}(l)}{(\pm\Omega-\Omega_\alpha)}\ , \tag{B9}$$

where Ω_α is an eigenvalue of the matrix $M(l,l')$. One sees early on that $G_{\pm}(l,l')$ satisfies

$$\pm\Omega G_{\pm}(l,l')-\sum_{l''}M(l,l'')G_{\pm}(l'',l')=\delta_{ll'}\ . \tag{B10}$$

The solution of Eq. (B4a) is then

$$S_{\pm}^{(1)}(l)=\tfrac{1}{2}\sum_\alpha\sum_{l'}\frac{e_L^{(\alpha)}(l')^* h(l')S(l')e_R^{(\alpha)}(l)}{\Omega_\alpha\mp\Omega}\ , \tag{B10a}$$

while the solution of Eq. (B4b) is

$$S_{\pm}^{(2)}(l)=\tfrac{1}{2}\sum_\alpha\sum_{l'}\frac{e_L^{(\alpha)}(l')^* h_x(l')S(l')e_R^{(\alpha)}(l)}{\Omega_\alpha\pm\Omega}\ . \tag{B10b}$$

If N_s is the number of spins in one layer of the superlattice (each layer is parallel to the xz plane), it is useful to perform a Fourier transform with respect to the variables l_x and l_z. Thus, $h_x(l)=h_x(l_x,l_y,l_z)$ is written as

$$h_x(l_x,l_y,l_z)=\frac{1}{(N_s)^{1/2}}\sum_{k_x,k_z}e^{ik_x l_x}e^{ik_z l_z}h_x(k_x,k_z;l_y)\ . \tag{B11}$$

The eigenvectors which emerge may also be written as

$$e_{R,L}^{(\alpha)}(l_x,l_y,l_z)=\frac{e^{ik_x l_x}e^{ik_z l_z}}{(N_s)^{1/2}}e_{R,L}^{(s)}(k_x,k_z;l_y)\ , \tag{B12}$$

where the index α which labels the eigenvalue is replaced on the right-hand side by the combination (k_x,k_z,s).

It is useful to switch the external perturbation on and off adiabatically by appending the factor $e^{\eta t}$ to each exponential in Eq. (B1). Then $S_{\pm}^{(1)}(l)$ and $S_{\pm}^{(2)}(l)$ may be written as

$$S_{\pm}^{(1)}(l)=\frac{1}{2(N_s)^{1/2}}\sum_s\sum_{l_y'}\sum_{k_x,k_z}\frac{e^{ik_x l_x}e^{ik_z l_z}\alpha^{(s)}(k_x,k_z;l_y,l_y')}{[\Omega_s(k_x,k_y)\mp\Omega+i\eta]} \tag{B13}$$

and

$$S_{\pm}^{(2)}(l)=\frac{1}{2(N_s)^{1/2}}\sum_s\sum_{l_y'}\sum_{k_x,k_z}\frac{e^{ik_x l_x}e^{ik_z l_z}\alpha^{(s)}(k_x,k_z;l_y,l_y')}{[\Omega_s(k_x,k_z)\pm\Omega\pm i\eta]}\ , \tag{B14}$$

where

$$\alpha^{(s)}(k_x,k_z;l_y,l_y')=e_L^{(s)}(k_x,k_z;l_y')^* h_x(k_x,k_z;l_y')S(l_y')e_R^{(s)}(k_x,k_z;l_y)\ . \tag{B15}$$

The above results may be used to derive an expression for $S_x(l,t)$, the $\hat{\mathbf{x}}$ component of spin at site l induced by the driving field. We find

$$S_x(l,t)=\frac{1}{2(N_s)^{1/2}}\sum_s\sum_{l_y'}\sum_{k_x,k_z}e^{ik_x l_x}e^{ik_z l_z}[e_L^{(s)}(k_x,k_z;l_y')]^* h_x(k_x,k_z;l_y')S(l_y')e_R^{(s)}(k_x,k_z;l_y)$$
$$\times\left[\frac{e^{\eta t}e^{i\Omega t}}{\Omega_s(k_x,k_z)-\Omega+i\eta}+\frac{e^{\eta t}e^{-i\Omega t}}{\Omega_s(k_x,k_z)+\Omega+i\eta}\right]\ . \tag{B16}$$

We can use Eq. (B16) to describe various quantities of physical interest. Consider, for example, the static susceptibility χ_{xx}, which describes the total transverse moment induced by a spatially uniform, time-independent field. We let $h_x(k_x,k_z;l_y')=(N_s)^{1/2}h_0\delta_{k_x,0}\delta_{k_z,0}$, so h_0 is the magnitude of the field felt by each spin. Then set $\Omega=\eta=0$, and if $\langle S_x\rangle$ is the average transverse moment per spin, with N the number of planes of spins in the unit cell,

$$\langle S_x\rangle=\frac{h_0}{N}\sum_{s=1}^{N}\sum_{l_y}\sum_{l_y'}\frac{[e_L^{(s)}(0,0;l_y')]^*S(l_y')e_R^{(s)}(0,0;l_y)}{\Omega_s(0,0)}\equiv\chi_{xx}h_0\ . \tag{B17}$$

The expression in Eq. (B17) was used to calculate the static susceptibilities displayed in Fig. 3.

If we wish to calculate the infrared absorption spectra, then the wavelength of the radiation will be long compared to the lattice constant, and also long compared to the period of the superlattice, at least for the structures of interest here. The energy per unit time absorbed by the system is proportional to

$$\frac{d\overline{W}}{dt}=\tfrac{1}{2}\sum_{l}\overline{h_x(l,t)dS_x(l,t)/dt}\ , \tag{B18}$$

where the vertical bar denotes an average over time. In the limit that the adiabatic switching parameter $\eta\to 0$, we find, per unit spin,

$$\frac{d\overline{W}}{dt}=\frac{\pi|h_x|^2\Omega}{128}\sum_{s}\sum_{l_y,l_y'}[\delta(\Omega-\Omega_s)-\delta(\Omega+\Omega_s)][e_L^{(s)}(l_y')]^*S(l_y')e_R^{(s)}(l_y)\ . \tag{B19}$$

In Eq. (B19), Ω_s stands for the spin-wave frequency $\Omega_s(k_x,k_z)$, evaluated with $k_x=k_z=0$, and in the eigenvectors we omit explicit reference to k_x and k_z. If we replace each δ function with a Lorentzian of width η, and then combine the two, Eq. (B19) becomes

$$\frac{d\overline{W}}{dt}=\frac{\Omega^2|h_x|^2}{32}\sum_{s}\frac{\Omega_s\eta}{[(\Omega_s^2-\Omega^2)^2+2\eta^2(\Omega^2+\Omega_s^2)]}\sum_{l_y,l_y'}[e_L^{(s)}(l_y')]^*S(l_y')e_R^{(s)}(l_y)\ . \tag{B20}$$

The calculations of the infrared absorption spectrum reported in the text use Eq. (B20), or the generalization of this expression to the more complex phases. In the numerical work, η has been chosen finite (and frequency independent) to crudely simulate the effect of damping.

We conclude with a brief sketch of the extension of the analysis to the unsymmetric and the superlattice spin-flop phases, where the spins are no longer aligned parallel or antiparallel to the z axis. We now write the equations of motion for the spin deviation operators $S'_{\pm}(l,t)$ introduced in Appendix A. These express the deviation of the spins away from the $\hat{\mathbf{z}}'$ axis, which is aligned along the direction of the spin at site l. We then seek solutions of the form $S'_{\pm}(l,t)=(S_{\pm}^{(1)})'(l)e^{i\Omega t}+(S_{\pm}^{(2)})'(l)e^{-i\Omega t}$, and then find that $(S_{\pm}^{(1)})'(l)$ obeys

$$\pm\Omega(S_{\pm}^{(1)})'(l)-\sum_{l'}M_1(l,l')S_{\pm}^{(1)}(l')-\sum_{l'}M_2(l,l')S_{\mp}^{(2)}(l')=-\tfrac{1}{2}h_x(l)\cos(\theta_{l_y})S\ , \tag{B21}$$

while $(S_{\pm}^{(2)})'(l)$ obeys an equation of the same structure, but with $\pm\Omega$ replaced by $\mp\Omega$. The matrices $M_1(l,l')$ and $M_2(l,l')$ are the same as those which enter the spin-wave theory described in Appendix A.

In this case, the variables $S_{+}^{(1,2)}(l)$ are coupled to $S_{-}^{(1,2)}(l)$, as in our theory of spin waves in the canted state. We proceed formally by introducing a vector,

$$\mathbf{S}^{(1,2)}=\begin{bmatrix}(S_{+}^{(1,2)})'(l_1)\\ \vdots\\ (S_{+}^{(1,2)})'(l_N)\\ (S_{-}^{(1,2)})'(l_1)\\ \vdots\\ (S_{-}^{(1,2)})'(l_N)\end{bmatrix}\ , \tag{B22}$$

and the eigenvalue problem defined by the homogeneous version of Eq. (B21) introduces eigenvalues Ω_α and left or right eigenvectors which we write as

$$\mathbf{e}_{R,L}^{(\alpha)}=\begin{bmatrix}e_{R,L}^{+(\alpha)}(l_1)\\ \vdots\\ e_{R,L}^{+(\alpha)}(l_N)\\ e_{R,L}^{-(\alpha)}(l_1)\\ \vdots\\ e_{R,L}^{-(\alpha)}(l_N)\end{bmatrix}\ . \tag{B23}$$

The orthonormality condition reads

$$\sum_{l}\{[e_L^{+(\alpha)}(l)]^*e_R^{+(\alpha')}(l)+[e_R^{-(\alpha)}(l)]^*e_R^{-(\alpha')}(l)\}=\delta_{\alpha\alpha'} \tag{B24}$$

and a similar generalization is made in the completeness relation stated earlier in Eq. (B7).

We may then expand the variables $(S_{\pm}^{(1)})'(l)$ and $(S_{\pm}^{(2)})'(l)$ in terms of the eigenvectors introduced in Eq. (B23), and we find

$$(S_{\pm}^{(1)})'(l)=\frac{S}{2}\sum_{\alpha}\sum_{l'}\frac{[e_L^{+(\alpha)}(l')-e_L^{-(\alpha)}(l')]^* h_x(l')\cos(\theta_{l_y'})e_R^{\pm(\alpha)}(l)}{\Omega_\alpha-\Omega}\ , \tag{B25a}$$

$$(S_{\pm}^{(2)})'(l)=\frac{S}{2}\sum_{\alpha}\sum_{l'}\frac{[e_L^{+(\alpha)}(l')-e_L^{-(\alpha)}(l')]^* h_x(l')\cos(\theta_{l_y'})e_R^{\pm(\alpha)}(l)}{\Omega_\alpha+\Omega}\ . \tag{B25b}$$

It is now a straightforward matter to generate expressions for various physical quantities of interest. For instance, after the introduction of a Lorentzian width η, one may show that the generalization of Eq. (B20) reads

$$\frac{d\overline{W}}{dt}=\frac{\Omega^2}{64}|h_x|^2\sum_s\frac{\Omega_s\eta}{[(\Omega_s^2-\Omega^2)^2+2\eta^2(\Omega_s^2+\Omega^2)]}$$
$$\times\sum_{l_y',l_y}[e_L^{+(s)}(l_y')-e_L^{-(s)}(l_y')]^* S\cos\theta_{l_y'}[e_R^{+(s)}(l_y)+e_R^{-(s)}(l_y)]\cos\theta_{l_y}\ . \tag{B26}$$

Because of the coupling between S_+ and S_- that occurs in the canted states, twice as many eigenvalues contribute to Eq. (B26) than contribute to Eq. (B20). One may show that the result in Eq. (B26) reduces to Eq. (B20), for the low-field ground state.

[1]A. Kueny, M. R. Khan, I. K. Schuller, and M. Grimsditch, Phys. Rev. B **29**, 2879 (1984).

[2]R. Damon and J. Eshbach, J. Phys. Chem. Solids **19**, 308 (1961).

[3]R. E. Camley, T. S. Rahman, and D. L. Mills, Phys. Rev. B **27**, 261 (1983).

[4]P. Grunberg and K. Mika, Phys. Rev. B **27**, 2955 (1983).

[5]K. Mika and P. Grunberg, Phys. Rev. B **31**, 4465 (1985).

[6]In practice, the spins in the ferromagnetic films will prefer to align parallel to the interfaces to avoid generating internal demagnetizing fields. Thus, we confine our attention to spin configurations of the superlattice for which all spins in each (100) plane are aligned parallel to each other and to the interfaces.

[7]Throughout this paper, we shall assume J_I is positive in sign. Our principle results, however, are insensitive to the sign of J_I, since changing its sign will simply reverse the moment of each ferromagnetic film. Then if the Zeeman field is applied antiparallel to the z direction, the energetics of various spin configurations is the same as considered here.

[8]F. B. Anderson and H. B. Callen, Phys. Rev. **136**, 1068 (1964).

[9]Y. Wang and H. B. Callen, J. Phys. Chem. Solids **25**, 1459 (1964).

[10]L. L. Hinchey and D. L. Mills, J. Appl. Phys. **57**, 3687 (1985).

[11]We consider classical spins (large S), and thus ignore distinction between $2KS$ and $2K(S-\frac{1}{2})$. The inclusion of the influence of quantum effects on the spin-wave dispersion relation is subtle, as the reader will appreciate from the comments on the results of Ref. 8 given in Sec. III of the present paper.

[12]C. Demangeat and D. L. Mills, Phys. Rev. B **14**, 4997 (1976); C. Demangeat, D. L. Mills, and S. E. Trullinger, *ibid.* **16**, 52 (1977); C. Demangeat and D. L. Mills, *ibid.* **16**, 2321 (1977).

[13]A complete discussion of the eigenvalue problem associated with non-Hermitian matrices is given by B. Friedman, *Principles and Techniques of Applied Mathematics* (Wiley, New York, 1956).

[14]In the absence of dipolar coupling, the Hamiltonian is invariant under rotations of the spin configuration about the axis, so we may choose to confine the spins in any plane we wish. As remarked in Ref. 6, in the presence of dipolar interactions, in those spin configurations where a transverse moment is present, the spins will lie in the plane parallel to the interfaces.

[15]C. Herring, Phys. Rev. **52**, 361 (1937) has discussed the influence of glide-plane symmetry on electron energy bands. Also, see the discussion that begins in C. Kittel, *Quantum Theory of Solids* (Wiley, New York, 1964), p. 213.